RSC Advances

ROYAL SOCIETY
OF CHEMISTRY

www.rsc.org/advances

Efficient titanium foil based perovskite solar cell: Using titanium dioxide nanowire arrays anode and transparent poly(3,4-ethylenedioxythiophene) electrode

Yaoming Xiao,[a,b,*] Gaoyi Han,[a,b] Haihan Zhou,[a,b] and Jihuai Wu[c]

[a]Institute of Molecular Science, Innovation Center of Chemistry and Molecular Science, Shanxi University, Taiyuan 030006, P. R. China.

[b]Key Laboratory of Materials for Energy Conversion and Storage of Shanxi Province, Taiyuan 030006, P. R. China.

[c]Institute of Materials Physical Chemistry, Huaqiao University, Quanzhou 362021, China.

[*] Corresponding author

E-mail: ymxiao@sxu.edu.cn (Yaoming Xiao).

Abstract: A titanium (Ti) foil based perovskite solar cell (PSC) is devised and prepared by employing titanium dioxide nanowire (TNW) arrays and titanium dioxide nanoparticles (TNPs) on the Ti foil substrates as the electron transporting layers (ETLs). The TNW array is desirable for the PSC, since it can provide direct pathways for the rapid collection and transmission of photo-generated electrons. The Ti foil substrate has many advantages such as flexibility, low sheet resistance, and excellent mechanical stability. The sunlight illuminates from a highly transparent poly(3,4-ethylenedioxythiophene) (PEDOT) film on the indium doped tin oxide/polyethylene naphthalate (ITO/PEN) substrate. The transparent PEDOT electrode can be

used as the hole transporting layer (HTL) due to the well matched band positions for the charge separation and transport. As a result, the Ti foil based light-weight PSC with the TNW arrays yields an efficiency of 13.07% with an active area of 1.00 cm^2, which is higher than that of the PSC with the TNPs (9.93%). These promising results highlight the potential application of the PEDOT and Ti foil in the cost-effective, large-area, and flexible PSC.

Keywords: poly(3,4-ethylenedioxythiophene), transparent electrode, titanium dioxide nanowire array, titanium foil, perovskite solar cell

Introduction

Organic-inorganic lead halide perovskite solar cells (PSCs) have garnered much interest as promising light harvesters for highly efficient photovoltaic devices in the past few years, due to their clean, low cost, high efficiency, good durability, and easy fabrication.[1-9] In a typical PSC, the fluorine doped tin oxide (FTO) coated glass is usually employed as a working electrode substrate to meet the requirement of preparing titanium dioxide (TiO_2) electron collection layer at high temperature (about 450 °C).[10] However, the heavy-weight and rigid glass substrate means low-cost manufacturing process (such as roll-to-roll processing[11]) is not possible. Therefore, fabrication of TiO_2 anodes on light-weight and flexible conductive substrates (such as polymer substrates and metal foils) has been investigated to realize a high-speed and low-cost manufacturing process of PSC modules.[12] Usually the polymer substrate can not be heated up to 150 °C, thus preparation of the PSC on it requires different approaches. There are some methods to fabricate the TiO_2 (electron collection and transport layer) on the polymer substrate: (1) low-temperature solution-processed method,[12-14] (2) atomic layer deposition,[15] and (3) replaced by other n-type materials (such as PCBM and polythiophene).[16,17]

Flexible metal foils (such as stainless steel and titanium (Ti) foil) have been widely used to fabricate flexible photovoltaic devices due to theirs flexibility, low sheet resistance, excellent thermal and mechanical stability. Flexible dye-sensitised solar cell based on Ti foil substrate was first demonstrated in 2006 by Ito et al.[18] and has garnered considerable attention from large-area solar cells.[19,20] Recently, L. Qiu, et al., prepared the PSC into a flexible stainless steel fiber with an energy conversion efficiency of 3.3%.[21] J. Troughton, et al., reported an efficiency of 10.3% for a flexible, ITO-free PSC using 150 mm thick Ti foil as a working electrode substrate.[22] The non-transparent metal foil in the PSC presents a different requirement to the transparent electrode to allow the backside sunlight illuminated from the transparent electrode side. Usually, the transparent polyaniline and poly(3,4-ethylenedioxythiophene) (PEDOT) electrodes have been widely used as the p-type hole transporting layers (HTLs) in the bifacial solar cells.[23-25]

Moreover, many efforts have been devoted to the design and synthesis of TiO_2 with particular structures to improve the photovoltaic performance of the TiO_2 anode.[26-28] The titanium dioxide nanowire (TNW) anode can provide direct pathways for the rapid collection and transmission of photo-generated electrons, which can improve the photovoltaic performance of the solar cell device.[29,30] Here we devised a Ti foil based light-weight PSC with TNW arrays and the sunlight illuminated from a highly transparent PEDOT film on the indium doped tin oxide/polyethylene naphthalate (ITO/PEN) substrate. Fig. 1 shows the device schematic diagram and energy level diagram of the light-weight PSC. The light-weight PSC yielded an average efficiency of 13.07%.

Experimental

Materials

3

Sodium hydroxide (NaOH), hydrochloric acid (HCl), hydrofluoric acid (HF), sodium dodecyl sulfate (SDS), lithium pechlorate (LiClO$_4$), lead iodide (PbI$_2$), hydroiodic acid (45 wt.% in water), methylamine (30% in methanol), methanol, ether, and acetonitrile were purchased from Shanghai Chemical Agent Ltd., China (Analysis purity grade). γ-butyrolactone (> 99.9%), ferrocene (> 99.9%), and tetrabutylammonium hexafluorophosphate (TBAPF$_6$, 98%) were purchased from Aladdin. 3,4-ethylenedioxythiophene monomer (EDOT) was purchased from Aldrich, USA. The above agents were used without further purification. Ti foil (> 99.98%, 0.05 mm thickness) was purchased from Baoji Yunjie Metal Production Co., Ltd. China.

Preparation of the light-weight anode

Typically, the TNW arrays were prepared on the flexible Ti foil to obtain the light-weight anode according to our reported procedure.[30] Firstly, Ti foil (1.0 cm × 2.5 cm) was cleaned in HF solution with a concentration of 0.03 mM for 2 min and rinsed in distilled water. Then the cleaned Ti foil was placed into Teflon-lined autoclave. Secondly, the autoclave was filled with 6 M NaOH solution (packing volume < 80%) and sealed into a stainless tank. Then the system was heated at 160 °C for 3 h. Thirdly, the obtained product was washed with HCl aqueous solution (pH = 2) and distilled water carefully until the pH value of the water equaled to 7. Finally, the product was sintered at 400 °C in air for 0.5 h.

Synthesis of the perovskite sensitizer solutions

The CH$_3$NH$_3$I was synthesized by a typical preparation procedure,[31,32] then the as-synthesized CH$_3$NH$_3$I powder (0.395 g) was mixed with PbI$_2$ (1.157 g) in γ-butyrolactone (3, 2, and 1 mL, respectively) at 60 °C for 12 h with stirring to obtain the three different concentrations of CH$_3$NH$_3$PbI$_3$/γ-butyrolactone solutions.

Electropolymerization of the PEDOT electrode

Before the plating, the flexible ITO/PEN substrates (12 $\pm$1 Ω sq^{-1}, Peccell, Japan) were cleaned with acetone and distilled water, respectively. The PEDOT was electrodeposited on the ITO/PEN substrate (1.0 cm $\times$ 2.5 cm) by the cyclic voltammetry (CV) measurement from an aqueous solution containing 10 mM SDS, 10 mM LiClO$_4$, and 2.0 mM EDOT under a three-electrode cell with a computer-controlled Autolab potentiostat (Type III) at ambient atmosphere.[19] The potential range was -0.1 V and 1.2 V for 15 cycles at a scan rate of 0.05 V s^{-1} for the PEDOT electropolymerization. Finally, the product was drying at 80 °C in a vacuum drying oven.

Fabrication of the solar cell

Two binder clips were used to assemble the PSC with the as-prepared light-weight TNW arrays based anode and PEDOT electrode in a sandwich-like architecture under an open system without any sealing (shown in the left side of **Fig. 1**). Then the three concentrations of $CH_3NH_3PbI_3$/γ-butyrolactone solutions were respectively injected into the PSCs from the gap between the two electrodes, and then dried in a vacuum oven at 100 °C for 12 h. The three PSCs were described as the PSC-b, PSC-c, and PSC-d, respectively. For comparison, the PSC based on the TiO$_2$ nanoparticles on the light-weight and flexible Ti foil was also prepared and named as the PSC-a. TiO$_2$ nanoparticle (TNP) slurry was prepared according to our previous reports,[19,33] and then coated on the Ti foil (cleaned by distilled water and acetone to retain the passive oxide film of TiO$_2$ as the dense blocking TiO$_2$ (DB-TiO$_2$)) by the spin-coating method at 500 r.p.m. for 10 s then at 6,000 r.p.m. for 30 s, then heat-treated at 400 °C for 0.5 h.

Characterizations and measurements

The Fourier transform infrared (FTIR) spectrum of the PEDOT was recorded on an Infrared Spectrometric Analyzer (BRUKER TENSOR 27) using KBr as pellets. The phase identification of the TNW, $CH_3NH_3PbI_3$ and TNW-$CH_3NH_3PbI_3$ was conducted with powder X-ray diffraction

(XRD, BRUKER D8-ADVANCE). The surface morphology of the sample was observed using a scanning electron microscopy (SEM, JEOL-JSM-6701F) operating at 10 kV. UV-Vis transmittance and absorption spectra of the samples were performed with an Agilent 8453 UV-Vis diode array spectrophotometer. The perovskite film was prepared on the bare ITO/PEN substrate for the UV-Vis transmittance and absorption measurement, and for the following CV test. CV test was carried out on a computer-controlled Autolab potentiostat (Type III) in a solution of $TBAPF_6$ (0.1 M) in anhydrous acetonitrile at a scan rate of 100 mV s at room temperature under argon protection. A platinum wire was used as the counter electrode. As a reference electrode (RE), a silver wire coated with AgCl was used. After each measurement, the RE was calibrated with ferrocene. The electrochemical impedance spectroscopy (EIS) of the PSC was performed using a CHI660D (Shanghai Chenhua Device Company, China) electrochemical measurement system at a constant temperature of 20 °C in ambient atmosphere under dark condition, and the impedance data covered a frequency range of 0.1 Hz to 10^5 Hz with 5 mV of amplitude and 0.9 V bias potential. The photocurrent density-voltage (J-V) characteristic of the PSC was carried out using a computer-controlled CHI660D from forward bias to short circuit (FB-SC) at 0.10 V s^{-1} in ambient atmosphere. The incident light intensity was set under 100 mW cm^{-2} (AM 1.5 G), and a black mask (1.00 cm^2) was used on top of the device to control the active cell area for the light irradiation. The incident monochromatic photon-to-current conversion efficiency (IPCE) curves were measured with a solar cell QE/IPCE measurement system (Solar Cell Scan 100, Beijing Zolix Instruments Co. Ltd., China).

Results and discussion

As the XRD patterns shown in **Fig. 2**, the characteristic diffraction peak at 2θ of 25.3º for titania

anatase (101) crystal face is observed in the pure TNW, and all sharp peaks can be indexed as titania anatase.[30] Strong diffraction peaks are observed at approximately 14.3, 20.1, 23.5, 24.5, 28.6, 31.8, 35.1, 40.5, and 43.3°, respectively corresponding to the reflections from (110), (112), (211), (202), (220), (310), (312), (224), and (314) crystal planes of the $CH_3NH_3PbI_3$ structure.[7,10,32,33] **Fig. S1** proves that the PEDOT thin film was successfully electropolymerized on the transparent ITO/PEN substrate by using the CV method.[19,34] The C-S bond stretching in the thiophene ring is found at 691 and 982 cm^{-1}. The vibrations at 1092, 1143 and 1204 cm^{-1} are possibility owing to C-O-C bond stretching in the ethylene dioxy group. The vibrations at 1339 and 1518 cm^{-1} can be attributed to the C-C and C=C stretching of the quinoidal structure of the thiophene ring.

    Fig. 3 a demonstrates three-dimensional interpenetrating network TNWs were successfully prepared on the Ti foil substrate through a facile hydrothermal approach. **Fig. 3** b-d represent the top-view SEM images of TNW arrays filled with three contents of $CH_3NH_3PbI_3$/γ-butyrolactone solutions on the Ti foil substrates. The $CH_3NH_3PbI_3$ could be well filled and contacted with the TNW arrays, and more $CH_3NH_3PbI_3$ was filled in the TNW arrays with the increase of its concentration. However, there is some break revealed in the perovskite film when the $CH_3NH_3PbI_3$ concentration is too high (**Fig. 3** d). **Fig. 3** e and f show the cross-sectional SEM images of the pure TNW arrays and TNW arrays filled with $CH_3NH_3PbI_3$ in 2 mL γ-butyrolactone. It can be seen that the TNW array grows tightly on the Ti foil substrate with a thickness of about 1000 nm, even though it has been went through a cutting process to prepare the SEM sample, and $CH_3NH_3PbI_3$ can be filled into the TNW arrays with a depth of 450 nm. **Fig. S2** presents that TNPs film is released easily from the Ti foil after the cutting process, suggesting the TNPs are not contacted strongly with the Ti foil substrate, and the $CH_3NH_3PbI_3$

only covers on the TNPs film. **Fig. S3** shows that the PEDOT film on the ITO/PEN substrate is homogeneous. After injected the perovskite sensitizer, the PEDOT film was covered with the $CH_3NH_3PbI_3$.

Fig. 4 shows the UV-Vis transmittance spectra of the $CH_3NH_3PbI_3$, PEDOT, and PEDOT-$CH_3NH_3PbI_3$ on the ITO/PEN substrates, respectively. The $CH_3NH_3PbI_3$ film has a low transmittance at around 470-770 nm and transmits weakly below 570 nm.[1,35] The transmittance at around 525-625 nm is observed for the PEDOT, which is assigned to π-π* electronic transition of the PEDOT.[36] Overall, the transmittance of the thin PEDOT film is quite high in the visible region. Thus, it can be considered as a visibly transparent electrode. Additionally, the curve of the PEDOT-$CH_3NH_3PbI_3$ exhibits superposed transmittance characteristics of the PEDOT and $CH_3NH_3PbI_3$ film. The broad absorption window overlapping with the maximum irradiance of the solar spectrum ensures efficient photon harvesting, which may eventually lead to a high photocurrent.

The optical band gap energy (E_g) of each material was calculated by using the equation of $E_g = 1240/\lambda$, in which the λ value was measured by the UV-Vis absorption spectra (**Fig. S4**). The highest occupied molecular orbital (HOMO) levels were estimated from the oxidation potential (E_{ox}) by using the empirical formulas of HOMO = - (E_{ox} + 4.80 - E_{ox}(Ferrocene)), in which the E_{ox} and E_{ox}(Ferrocene) values were measured by the cyclic voltammetry (**Fig. S5**), and the lowest unoccupied molecular orbital (LUMO) levels were calculated according to the equation of LUMO = HOMO + E_g.[33] The results were listed in **Table 1**. **Fig. 1** (the right side) shows the energy level diagram of the TNW, $CH_3NH_3PbI_3$, and PEDOT, respectively, where all the band positions are well matched for the charge separation and directional transport. In the photoelectric conversion process, the sunlight illuminates from the highly transparent PEDOT

electrode, the $CH_3NH_3PbI_3$ absorbs the photon at its interface, then charge separation occurs at the interface and quickly transfers to the conductive band (CB) of the semiconductor TNW arrays, finally forms the photo-current by the external circuit. In this structure, the TNW arrays can provide direct pathways for the rapid collection and transmission of photo-generated electrons. Moreover, the LUMO level of the PEDOT is higher than that of the $CH_3NH_3PbI_3$, which can lead to a single directional pathway for the photon-generated electron transport to reduce the electron recombining to the PEDOT.

Table 1 Optical and electrochemical properties of the TNW, $CH_3NH_3PbI_3$, and PEDOT, respectively.

Sample	λ^a	E_g^b	E_{ox}^c	E_{ox}(Ferrocene)	HOMO^d	LUMO^e
	(nm)	(eV)	(V)	(V)	(eV)	(eV)
TNW	383	3.24	3.15	0.42	-7.53	-4.29
$CH_3NH_3PbI_3$	825	1.50	1.00	0.42	-5.38	-3.88
PEDOT	565	2.19	0.73	0.42	-5.11	-2.92

^{a} λ measured by UV-Vis absorption spectra (**Fig. S4**); ^{b} E_g = 1240/λ;

^{c} Oxidation potentials measured by cyclic voltammetry (**Fig. S5**); ^{d} HOMO = - (E_{ox} + 4.80 - E_{ox}(Ferrocene)) eV;

^{e} LUMO = HOMO + E_g

The internal resistance of the photovoltaic device is usually characterized by EIS, as shown in **Fig. 5** a, and the equivalent circuit of this model (inset of **Fig. 5** a) has been already reported.[7,10,32,33,37] In which the R_S refers to the ohmic series resistance, the R_{CT}(PEDOT) and R_{CT}(TNW) are the charge-transfer resistance at the PEDOT/$CH_3NH_3PbI_3$ and $CH_3NH_3PbI_3$/TNW interface, the Y_{CPE}(PEDOT) and Y_{CPE}(TNW) refer to the constant phase elements. The resultant impedance spectra were fitted using the Z-view software and shown in **Table 2**. It can be seen that the R_S, R_{CT}(TNW), and R_{CT}(PEDOT) values of the TNW arrays based PSCs (PSC-b, PSC-c,

and PSC-d) are observably lower than those of the TiO_2 nanoparticles based PSC (PSC-a), owing to that the TNW arrays have more excellent electron transport ability than that of the TiO_2 nanoparticles, which can provide direct pathways for the rapid collection and transmission of photo-generated electrons. And these values of the TNW arrays based PSCs are gradually reduced by injecting more $CH_3NH_3PbI_3$ into the device, owing to the high carrier mobility of the $CH_3NH_3PbI_3$ were filled up in both the TNW and PEDOT films. However, an excess of $CH_3NH_3PbI_3$ in the device brings about some break in the perovskite film, which could result in a disadvantage of the electron transport. The lowest R_S, R_{CT}(TNW), and R_{CT}(PEDOT) values of the PSC-c are 13.15, 54.25, and 24.22 Ω cm^2, respectively. The lower resistances could result in a more effective and rapid transporting ability for the electron and hole, which would further improve the performance of the PSC especially the fill factor.

Table 2 EIS results of the light-weight PSCs under dark condition.

Device	R_S	R_{CT}(TNW)	Y_{CPE}(TNW)	R_{CT}(PEDOT)	Y_{CPE}(PEDOT)
	(Ω cm^2)	(Ω cm^2)	(mF cm^{-2})	(Ω cm^2)	(mF cm^{-2})
PSC-a	16.91	78.13	0.91	40.48	0.81
PSC-b	14.25	61.82	0.97	29.26	0.79
PSC-c	13.15	54.25	0.99	24.22	0.82
PSC-d	13.40	59.16	0.99	25.70	0.80

The photovoltaic properties of light-weight PSCs were measured using a computer-controlled CHI660D from forward bias to short circuit (FB-SC) at 0.10 V s^{-1} under full sunlight illumination (100 mW cm^{-2}, AM 1.5 G) from the PEDOT electrode side (**Fig. 5** b), and the average results were summarized in **Table 3**. The short-circuit current density (J_{SC}), open-circuit voltage (V_{OC}), and fill factor (*FF*) values of the light-weight PSC-c are observably

enhanced by introducing the TNW arrays into the solar cell and employing moderate amounts of $CH_3NH_3PbI_3$. The light-weight PSC-a based on TiO_2 nanoparticles yields an efficiency of 9.93%. However, the light-weight PSC-c with TNW arrays yields an increased efficiency of 13.07%. The enhanced J_{SC} might be owing to the high specific surface area of the TNW arrays and enough $CH_3NH_3PbI_3$ to increase the utilization of sunlight. The increased V_{OC} might be due to the array structure of the TNW to provide direct pathways for the rapid collection and transmission of photo-generated electrons. The FF value of the PSC-c is enhanced by employing the TNW arrays, attributing to the decreased values of the R_S, R_{CT}(TNW), and R_{CT}(PEDOT).

Table 3 The photovoltaic performances of the light-weight PSCs under full illumination (100 mW cm^{-2}, AM 1.5 G).

PSC	J_{SC} (mA cm^{-2})	V_{OC} (V)	FF	η (%)
PSC-a	18.71 ± 0.06	0.87 ± 0.04	0.61 ± 0.02	9.93 ± 0.05
PSC-b	19.89 ± 0.06	0.91 ± 0.04	0.62 ± 0.02	11.22 ± 0.05
PSC-c	21.72 ± 0.06	0.94 ± 0.04	0.64 ± 0.02	13.07 ± 0.05
PSC-d	20.84 ± 0.06	0.94 ± 0.04	0.63 ± 0.02	12.34 ± 0.05

Fig. 6 shows more photovoltaic performances based on the best device of PSC-c. **Fig. 6** a provides the statistics distribution on the reproducibility of the PSC-c efficiencies. The average efficiency is about 13.07% scanned from forward bias to short circuit at 0.10 V s^{-1}. IPCE curve shows a wide light response across the whole visible spectrum (**Fig. 6** b), and the integrated current density from the IPCE is about 20.19 mA cm^{-2}, which is lower than that of the measured value of 21.72 mA cm^{-2}. This is due to that there is some mismatch between the simulated sunlight and AM1.5G standard. The hysteresis behavior is universally present in the solar cell when the current-voltage curve is diminished at low scanning rate.[38] **Fig. 6** c shows the PSC-c

yielded efficiencies of 13.07% and 7.27% based on the scanning directions from forward bias to short circuit (FB-SC) and from short circuit to forward bias (SC-FB), respectively. The average efficiency is about 10.17% from the two current-voltage curves. Because of the device was measured under an open system without any sealing in ambient atmosphere, decreasing values of the J_{SC}, V_{OC}, and η are observed in **Fig. 6** d under total scan time 400 s. However, 83.75%, 94.15%, and 78.81% of the initial values of the J_{SC}, V_{OC}, and η are retained after scanning 400 s taking no account of the change of the fill factor.

Conclusions

In summary, the TNW arrays were introduced as the electron collection layer for the light-weight PSC, which provided direct pathways for the rapid collection and transmission of photo-generated electrons, resulting in a low resistances to enhance the PSC performance. The $CH_3NH_3PbI_3$ could be well filled with a depth of 450 nm into the TNW arrays. The highly transparent PEDOT acted as the HTL due to well matched band positions for the charge separation. The low-cost and light-weight PSC based on the TNW arrays yielded an efficiency of 13.07% with an active area of 1.00 cm^2. The present work suggests that the Ti foil and PEDOT show a great potential as a cost-effective substrate and HTL for the large-area, light-weight and flexible photovoltaic device.

Acknowledgments

References

1   M. Lee, J. Teuscher, T. Miyasaka, T. Murakami and H. Snaith, *Science*, 2012, **338**, 643-647.

2   J. Burschka, N. Pellet, S. Moon, R. Humphry-Baker, P. Gao, M. Nazeeruddin and M. Grätzel, *Nature*, 2013, **499**, 316-319.

3   M. Liu, M. Johnston and H. Snaith, *Nature*, 2013, **501**, 395-398.

4   A. Mei, X. Li, L. Liu, Z. Ku, T. Liu, Y. Rong, M. Xu, M. Hu, J. Chen, Y. Yang and M. Grätzel, H. Han, *Science*, 2014, **345**, 295-298.

5   H. Zhou, Q. Chen, G. Li, S. Luo, T. Song, H. Duan, Z. Hong, J. You, Y. Liu and Y. Yang, *Science*, 2014, **345**, 542-546.

6   Y. Wu, A. Islam, X. Yang, C. Qin, J. Liu, K. Zhang, W. Peng and L. Han, *Energy Environ. Sci.*, 2014, **7**, 2934-2938.

7   Y. Xiao, G. Han, Y. Li, M. Li and J. Wu, *J. Mater. Chem. A*, 2014, **2**, 16856-16862.

8   D. deQuilettes, S. Vorpahl, S. Stranks, H. Nagaoka, G. Eperon, M. Ziffer, H. Snaith and D. Ginger, *Science*, 2015, **348**, 683-686.

9   N. Jeon, J. Noh, W. Yang, Y. Kim, S. Ryu, J. Seo and S. Seok, *Nature*, 2015, **517**, 476-480.

10   Y. Xiao, G. Han, Y. Li, M. Li, Y. Chang and J. Wu, *J. Mater. Chem. A*, 2014, **2**, 16531-16537.

11   M. Biancardo, K. West and F. Krebs, *Sol. Energ. Mater. Sol. Cells*, 2006, **90**, 2575-2588.

12   J. Jung, S. Williams and A. Jen, *RSC Adv.*, 2014, **4**, 62971-62977.

13   P. Docampo, J. Ball, M. Darwich, G. Eperon and H. Snaith, *Nature Commun.*, 2013, **4**,

2761.

14   Y. Dkhissi, F. Huang, S. Rubanov, M. Xiao, U. Bach, L. Spiccia, R. Caruso and Y. Cheng, *J. Power Sources*, 2015, **278**, 325-331.

15   B. Kim, D. Kim, Y. Lee, H. Shin, G. Han, J. Hong, K. Mahmood, T. Ahn, Y. Joo, K. Hong, N. Park, S. Lee and H. Jung, *Energy Environ. Sci.*, 2015, **8**, 916-921.

16   J. You, Z. Hong, Y. Yang, Q. Chen, M. Cai, T. Song, C. Chen, S. Lu, Y. Liu, H. Zhou and Y. Yang, *ACS Nano*, 2014, **8**, 1674-1680.

17   W. Yan, Y. Li, W. Sun, H. Peng, S. Ye, Z. Liu, Z. Bian and C. Huang, *RSC Adv.*, 2014, **4**, 33039-33046.

18   S. Ito, N. Ha, G. Rothenberger, P. Liska, P. Comte, S. Zakeeruddin, P. Péchy, M. Nazeeruddin and M. Grätzel, *Chem. Commun.*, 2006, **38**, 4004-4006.

19   J. Wu, Y. Xiao, G. Yue, Q. Tang, J. Lin, M. Huang, Y. Huang, L. Fan, Z. Lan, S. Yin and T. Sato, *Adv. Mater.*, 2012, **24**, 1884-1888.

20   Y. Xiao, J. Wu, G. Yue, J. Lin, M. Huang, L. Fan and Z. Lan, *J. Power Sources*, 2012, **208**, 197-202.

21   L. Qiu, J. Deng, X. Lu, Z. Yang and H. Peng, *Angew. Chem. Int. Ed.*, 2014, **53**, 1-5.

22   J. Troughton, D. Bryant, K. Wojciechowski, M. Carnie, H. Snaith, D. Worsley and T. Watson, *J. Mater. Chem. A*, 2015, **3**, 9141-9145.

23   Q. Tai, B. Chen, F. Guo, S. Xu, H. Hu, B. Sebo and X. Zhao, *ACS Nano*, 2011, **5**, 3795-3799.

24   P. You, Z. Liu, Q. Tai, S. Liu and F. Yan, *Adv. Mater.*, 2015, **27**, 3632-3638.

25   K. Sun, P. Li, Y. Xia, J. Chang and J. Ouyang, *ACS Appl. Mater. Interfaces*, 2015, **7**, 15314-15320.

26   Z. Miao, D. Xu, J. Ouyang, G. Guo, X. Zhao and Y. Tang, *Nano Lett.*, 2002, **2**, 717-720.

27   X. Zhang, Z. Bao, X. Tao, H. Sun, W. Chen and X. Zhou, *RSC Adv.*, 2014, **4**, 64001-64005.

28   P. Qin, M. Paulose, M. Dar, T. Moehl, N. Arora, P. Gao, O. Varghese, M. Grätzel and M. Nazeeruddin, *Small*, 2015, DOI: 10.1002/smll.201501460.

29   X. Feng, K. Shankar, M. Paulose and C. Grimes, *Angew. Chem.*, 2009, **48**, 8095-8098.

30   Y. Xiao, J. Wu, G. Yue, J. Lin, M. Huang, L. Fan and Z. Lan, *RSC Adv.*, 2012, **2**, 10550-10555.

31   J. Heo, S. Im, J. Noh, T. Mandal, C. Lim, J. Chang, Y. Lee, H. Kim, A. Sarkar, M. Nazeeruddin, M. Grätzel and S. Seok, *Nature Photon.*, 2013, **7**, 487-492.

32   Y. Xiao, G. Han, Y. Chang, Y. Zhang, Y. Li and M. Li, *J. Power Sources*, 2015, **286**, 118-123.

33   Y. Xiao, G. Han, Y. Chang, H. Zhou, M. Li and Y. Li, *J. Power Sources*, 2014, **267**, 1-8.

34   Y. Xiao, J. Lin, S. Tai, S. Chou, G. Yue and J. Wu, *J. Mater. Chem.*, 2012, **22**,

35   Y. Zhao and K. Zhu, *J. Phys. Chem. Lett.*, 2013, **4**, 2880-2884.

36   X. Zhang, A. MacDiarmid and S. Manohar, *Chem. Commun.*, 2005, **42**, 5328-5330.

37   Y. Zhao, J. Zhai, T. Wei, L. Jiang and D. Zhu, *J. Mater. Chem.*, 2007, **17**, 5084-5089.

38   H. Snaith, A. Abate, J. Ball, G. Eperon, T. Leijtens, N. Noel, S. Stranks, J. Wang, K. Wojciechowski, and W. Zhang, *J. Phys. Chem. Lett.*, 2014, **5**, 1511-1515.

Figure Captions

Fig. 1 Device schematic diagram (the left side) and energy level diagram (the right side) of the light-weight PSC.

Fig. 2 XRD patterns of the TNW, $CH_3NH_3PbI_3$, and TNW-$CH_3NH_3PbI_3$, respectively.

Fig. 3 Top-view SEM images of the pure TNW arrays (a), TNW-$CH_3NH_3PbI_3$ based on 3 (b), 2 (c), and 1 (d) mL γ-butyrolactone, respectively; Cross-sectional SEM images of the pure TNW arrays (e) and TNW-$CH_3NH_3PbI_3$ (f), respectively; All SEM images with a bar of 100 nm.

Fig. 4 UV-Vis transmittance spectra of the $CH_3NH_3PbI_3$, PEDOT, and PEDOT-$CH_3NH_3PbI_3$ on the ITO/PEN substrates, respectively.

Fig. 5 Nyquist plots of the light-weight PSCs under dark condition (a) and photocurrent density-voltage characteristics of the light-weight PSCs under full illumination (b).

Fig. 6 Statistics distribution of the PSC-c efficiencies with ten cells prepared under the same conditions, error bars represent minimum and maximum values, and the middle line in each box represents the median value (a); IPCE curve of the PSC-c (b); Forward bias to short circuit (FB-SC) and short circuit to forward bias (SC-FB) current-voltage curves measured under AM1.5 simulated sun light for the PSC-c, the inset table gives the FB-SC, SC-FB, and average performance parameters (c); Short-circuit current density (J_{SC}) as a function of time for the PSC-c held close to 0.94 V forward bias under dark condition (black line), open-circuit potential (V_{OC}) as a function of time for the PSC-c under AM1.5 simulated sun light (blue line), power conversion efficiency (η) as a function of time calculated by the equation: η (%) = ($J_{SC} \times V_{OC} \times 0.64$)%, in which 0.64 is the fill factor (red line) (d).
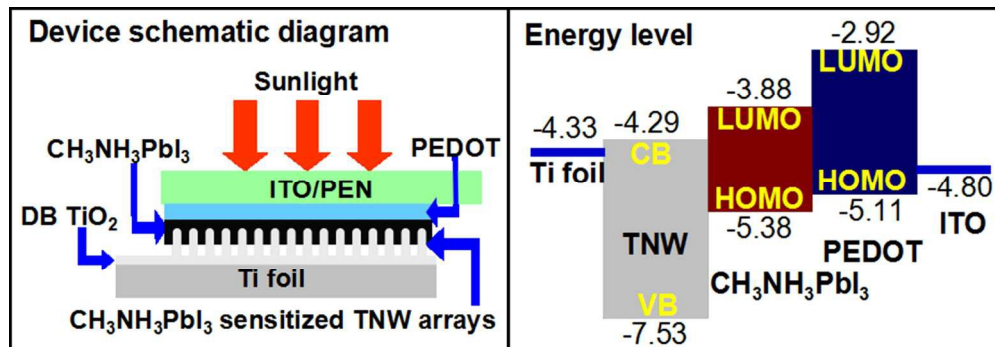
244x85mm (96 x 96 DPI)
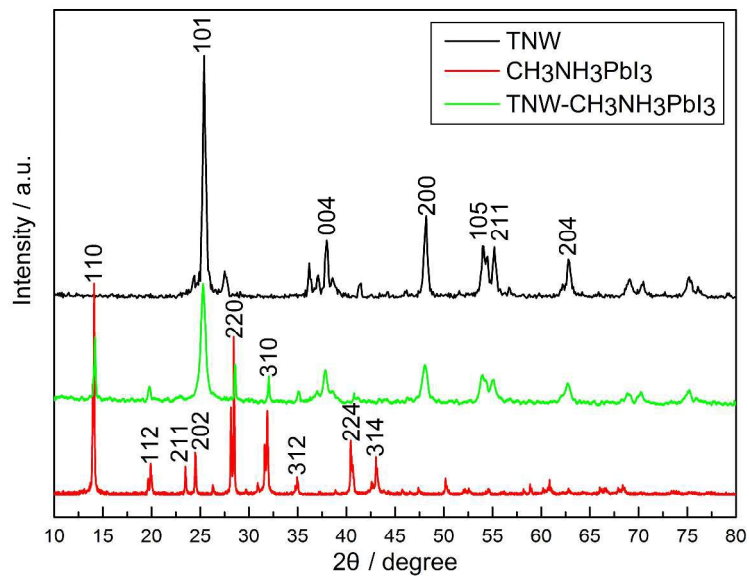
1188x840mm (150 x 150 DPI)
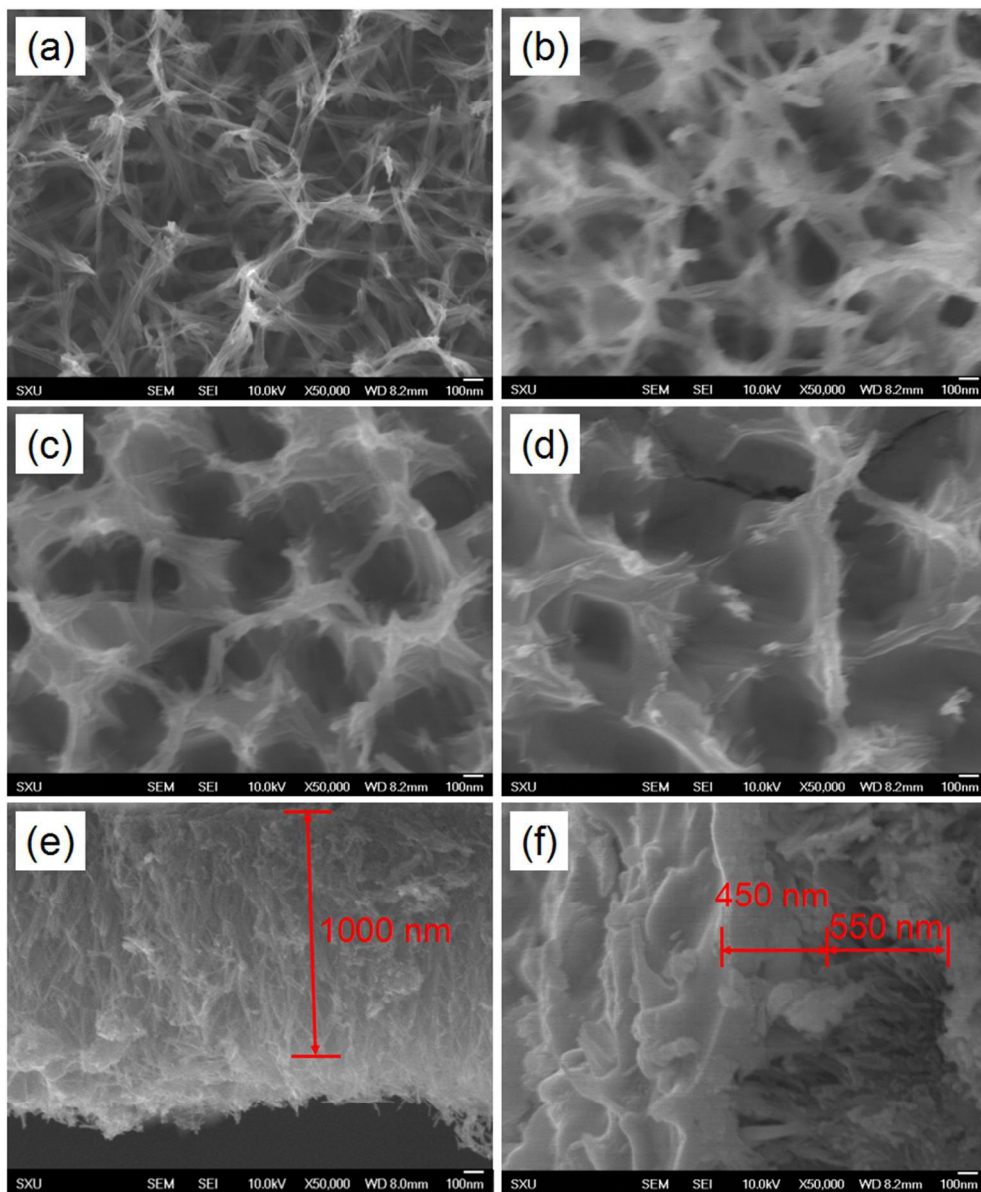
246x296mm (96 x 96 DPI)
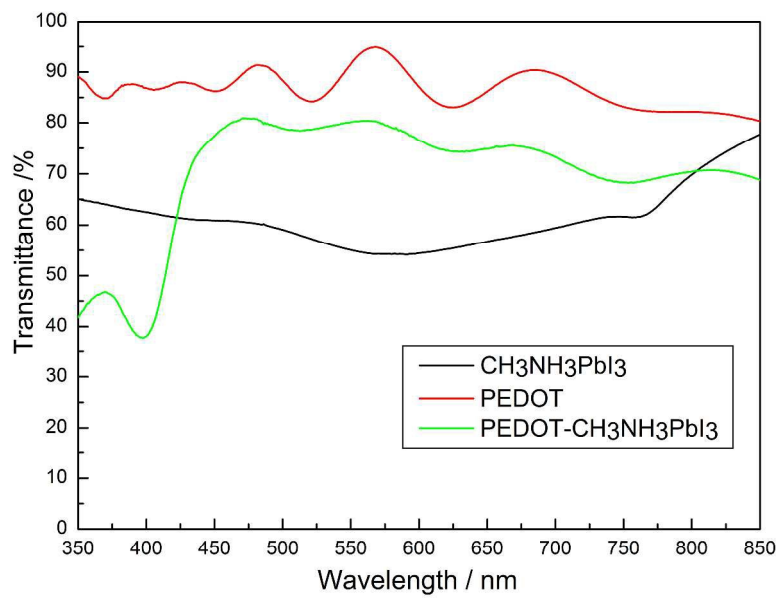
1188x840mm (150 x 150 DPI)
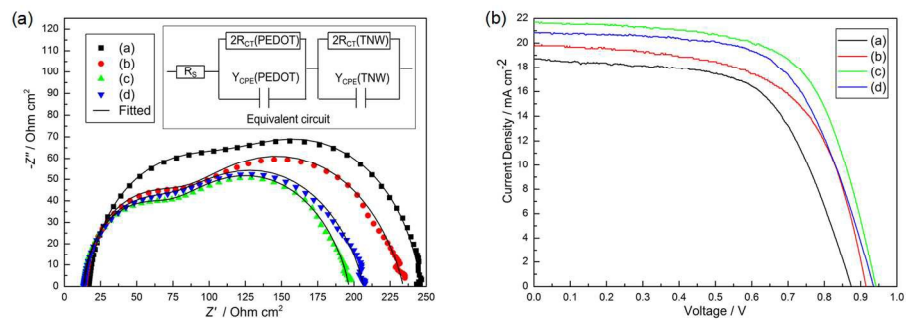
478x179mm (96 x 96 DPI)
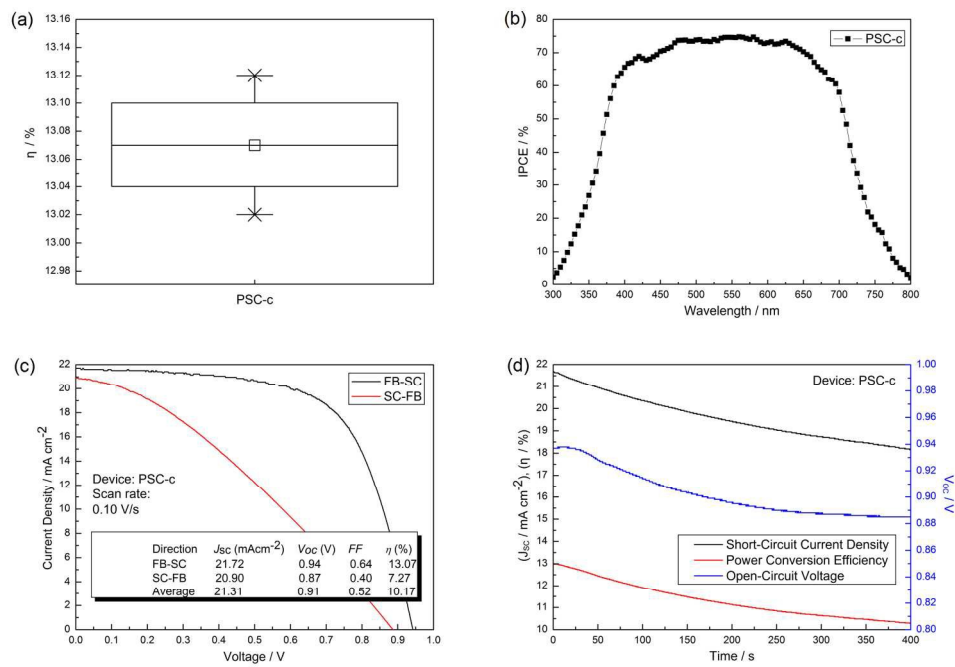
533x381mm (96 x 96 DPI)

An efficient and light-weight perovskite solar cell (PSC) is devised and prepared by employing titanium dioxide nanowire (TNW) arrays on the Ti foil substrate as the electron collection layer and using a highly transparent PEDOT on the ITO/PEN substrate as the hole transporting layer. As a result, the light-weight PSC based on the TNW arrays yields an efficiency of 13.07%, which is higher than that of the PSC without the TNW arrays (9.93%). These promising results highlight the potential application of the Ti foil in the cost-effective, large-area and flexible PSC.